Applied Catalysis B: Environmental 232 (2018) 101–107

Contents lists available at ScienceDirect

Applied Catalysis B: Environmental

journal homepage: www.elsevier.com/locate/apcatb

Conversion of hemicellulose-derived pentoses over noble metal supported on 1D multiwalled carbon nanotubes

Rafael F. Perez[a,b], Olivia S.G.P. Soares[c], Andréa M. Duarte de Farias[a], M. Fernando R. Pereira[c,**], Marco A. Fraga[a,b,*]

[a] Instituto Nacional de Tecnologia/MCTIC, Divisão de Catálise e Processos Químicos, Av. Venezuela, 82/518, Saúde, 20081-312, Rio de Janeiro, Brazil
[b] Instituto Militar de Engenharia, Praça Gen. Tibúrcio, 80, Urca, 2290-270, Rio de Janeiro, Brazil
[c] Laboratório de Processos de Separação e Reacção – Laboratório de Catálise e Materiais (LSRE-LCM), Dept. Eng. Química, Faculdade de Engenharia, Universidade do Porto, R. Dr. Roberto Frias, 4200-465, Porto, Portugal

ARTICLE INFO

Keywords:
Xylose
Xylitol
Furfuryl alcohol
Aqueous-phase processing
Biorefinery
Lignocellulosic biomass
Nanocatalyst

ABSTRACT

Conversion of xylose was investigated over noble metals supported on multiwalled carbon nanotubes (MWCNT). Distinct metal nanoparticles were dispersed on functionalized MWCNT bearing acidic groups created by HNO_3 oxidation and their catalytic performance and stability on aqueous-phase processing of pentoses were assessed. While oxidized MWCNT exhibited low activity to dehydration products, noble metal-based one-dimensional catalysts showed to be much more active. Ru decorated MWCNT was by far the most active catalyst with total xylose consumption within the first 1.5 h. Rh and Au supported samples could barely accomplish 40% conversion after 6 h. The activity order Ru > > Pd > Pt > Rh ~ Au could be established among the studied samples. Xylitol derived from direct hydrogenation of pentoses was invariably the key product formed, accomplishing selectivities within 70–85%. It revealed that the metal centers were mostly acting independently. Furfuryl alcohol was the second major product and its formation was well correlated to the concentration of acidic surface sites created upon MWCNT oxidation, evidencing a cooperative role between metal and acidic sites. The oxygenated surface groups of fresh and spent catalysts assessed by TPD were shown to be stable under the aqueous-phase processing conditions used.

1. Introduction

Lignocellulosic biomass potentially plays a central role in the development of a sustainable economy due to its large availability as a by-product of active industrial sectors in many countries. The three carbon-based fractions of lignocellulosic biomass – cellulose, hemicellulose and lignin – stand as the most valuable renewable organic carbon sources to replace oil. Their valorization goes from second-generation biofuel production to a wide range of bio-based green chemicals, establishing the basis for the widespread biorefinery concept. These processes, however, require special attention due to the high reactivity and low volatility of second-generation sugars and other biomass-derived compounds. Therefore, catalytic conversion of sugars to other high valued green chemicals is performed at low temperatures and in aqueous phase.

Aqueous-phase processing (APP) brings some technical challenges, particularly regarding the structure of the heterogeneous catalyst. It has been shown, for instance, that γ-alumina [1,2] and some zeolites [3] can be vulnerable as a catalyst or catalyst support for APP since significant physico-chemical changes upon reaction in water can take place. Other oxides, as zirconia, on the other hand, have been successfully exploited for such purpose [4].

Amongst potential materials, carbon-based ones can be easily pinpointed. One-dimensional (1D) carbon nanotubes (CNTs), in particular, have demonstrated excellent abilities to replace conventional catalyst supports in heterogeneous catalysis owing to their remarkable properties like high electrical conductivity, mechanical and thermal stabilities; tolerance against poisoning and the possibility of tuning their textural and chemical surface properties [5,6]. An additional advantage is related to the fact that they can be applied as an agglomerate of tubes acting as a mesoporous material, with the metal active sites on the external walls of the tubes, avoiding the usual mass transfer limitations found in porous materials [7]. The catalytic activity of the supported catalysts depends significantly on the distribution of the active sites on the support. Moreover, the nature of the supports, like their surface chemical properties, also influences the catalytic activity and selectivity

* Corresponding author at: Instituto Nacional de Tecnologia/MCTIC, Divisão de Catálise e Processos Químicos, Av. Venezuela, 82/518, Saúde, 20081-312, Rio de Janeiro, Brazil.
** Corresponding author.
E-mail addresses: fpereira@fe.up.pt (M.F. R. Pereira), marco.fraga@int.gov.br (M.A. Fraga).

https://doi.org/10.1016/j.apcatb.2018.03.042
Received 6 August 2017; Received in revised form 1 December 2017; Accepted 14 March 2018
Available online 16 March 2018

[8]. The interaction of the support with the active sites as well as with the reaction reactants and products can be modified by tailoring their textural and chemical surface properties [9,10]. In this sense, oxygen-containing groups can be introduced on the CNT surface by controlled oxidation conditions. The functionalization with nitric acid, for example, can introduce large amounts of carboxylic acids and also some lactones, carboxylic anhydrides, phenols and carbonyl-quinones on the CNT surface [11]. These groups can be used to anchor catalyst precursors or for subsequent functionalization. In addition, they may be active sites for specific catalytic reactions, since they hold an acidic or basic character depending on their chemical nature, or constitute a bifunctional system along with metal nanoparticles dispersed on it.

Xylose is the main hemicellulosic pentose sugar released from lignocellulosic biomass and is industrially used for obtaining furfural, furfuryl alcohol and xylitol. This later compound is an alternative sweetener with rising importance in food industry and increasing global production. Furfuryl alcohol, on the other hand, is a key intermediate for the production of valuable chemicals among them levulinic acid can be mentioned. Driving the catalytic transformation of xylose to any of the above-mentioned products is a matter of tailoring the catalyst surface, mainly the generation and distribution of metal and acidic surface centers [12–14]. Indeed, xylose hydrogenation to xylitol occurs on metal sites [13] while one-pot production of furfuryl alcohol would demand vicinal acid and metal sites to promote the tandem xylose dehydration-furfural hydrogenation reactions [12,14]. Such a balance between sites may not be a simple task though.

In this contribution, 1D multiwalled carbon nanotubes (MWCNT)-supported noble metal (Pt, Pd, Ru, Rh and Au) catalysts were evaluated on xylose conversion in aqueous phase. The chemoconversion of pentoses was investigated over bifunctional heterogeneous catalysts bearing both those noble metal sites and acidic centers generated by oxygen functionalization. The potential interplay between these sites is reported and discussed aiming at contributing to a better understanding of a bifunctional catalyst design for biomass conversion.

2. Experimental

Commercially available multiwalled carbon nanotubes with the reference Nanocyl 3100 were functionalized by refluxing with nitric acid (7 mol L^{-1}) at 130 °C for 3 h, followed by washing, filtering and drying (MWCNT). This 1D nanostructured support was impregnated, by the incipient wetness impregnation method, with noble metal (Pt, Pd, Ru or Rh) using the salt precursors H_2PtCl_6, $PdCl_2$, $RuCl_3$, $RhCl_3$ or $HAuCl_4$, respectively, purchased from Alfa Aeser, to obtain 1 wt.%. After, they were thermal treated at 200 °C for 1 h under N_2 and finally reduced at 100 °C under H_2 for 3 h. The Au/MWCNT sample was synthesized by a colloidal method [15], calcined at 350 °C for 1 h and then reduced at 350 °C for 3 h.

Due to the preparation method used, the amount of each metal is expected to be very close to the nominal value (1 wt.%). To confirm it, sample Pd/MWCNT was characterized by ICP-AES in a Jobin Yvon Activa-M equipment and the amount of metal obtained was 0.98 wt.%.

Nanostructured catalysts were characterized as regarding their surface area by N_2 physisorption (S_{BET}) and their acid properties by titration (pH_{PZC}). Identification of functional groups was accomplished by thermoprogrammed decomposition (TPD) and their vibrational characteristics were assessed by laser Raman spectroscopy (LRS). Morphology and metal nanoparticles dispersion were examined by transmission electron microscopy (TEM).

The textural characterization of the catalysts and supports was based on the corresponding N_2 adsorption isotherms, determined at −196 °C with Nova 4200e (Quantachrome Instruments) equipment.

The pH_{PZC} was determined by the drifts method. 50 cm^3 of NaCl 0.01 mol L^{-1} solution was placed in a closed Erlenmeyer flask, the pH was adjusted to a value between 2 and 12 by adding HCl 0.1 mol L^{-1} or NaOH 0.1 mol L^{-1} solutions ($pH_{initial}$). Then, 0.15 g of the MWCNT sample was added to each flask and the final pH was measured after 48 h under agitation at room temperature (pH_{final}). The pH_{PZC} is the point where the curve pH_{final} vs. pH_{inital} crosses the line $pH_{initial} = pH_{final}$.

CO and CO_2 TPD profiles were obtained with a fully automated AMI-300 equipment (Altamira Instruments). The samples (100 mg) were heated (5 °C min^{-1}) up to 1100 °C under a flow rate of 25 cm^3 min^{-1} of helium. The amounts of CO ($m/z = 28$) and CO_2 ($m/z = 44$) released from the samples were followed by mass spectrometry (Dymaxion 200, Ametek). For quantification of the CO and CO_2 released, calibration of these gases was carried out at the end of each analysis.

The structure of the 1D nanocatalysts were analyzed by using a Raman spectrometer Horiba Jobin Yvon LabRam equipped with a 633 nm laser and a CCD detector operating at −70 °C. Spectra were collected with resolution of 1800 lines/mm. The ratios between D and G Raman bands (D/G) were determined by calculating their areas in the spectra. A deconvolution treatment was applied to distinguish all contributions. Typically, the spectra were decomposed into four Lorentz components as shown in a representative spectrum in Fig. S5 in the Supporting information.

Morphology and metal nanoparticles dispersion were examined by transmission electron microscopy (TEM) in a FEI Tecnai microscope, operating at 200 kV. Before the analyses, the catalysts were ultrasonically dispersed on 2-propanol and deposited on a carbon-coated copper grid.

Pentose conversion was evaluated in a three-phase semi batch PARR reactor at 130 °C and 30 bar H_2, using H_2O:2-propanol (1:1) as solvent mixture and xylose initial concentration of 83 mmol L^{-1} [12,14]. These conditions were shown to avoid diffusional limitations and any contribution from thermoconversion of xylose [16].

Catalytic runs were performed for 6 h and samples were taken periodically to follow the reaction kinetics. These aliquots were analysed by HPLC in a Waters Alliance e2695 equipment coupled to a refractive index detector (RID) kept at 50 °C. Analyses were carried with the aid of a Biorad Aminex HPX-87H ion exchange column at 65 °C, using a H_2SO_4 5 mmol L^{-1} solution at 0.7 mL min^{-1} as mobile phase on isocratic mode.

After liquid-phase reaction, the nanocatalysts were collected by filtration, dried overnight at 100 °C and finally characterized by LRS and TPD in order to assess eventual changes in their most standard features. The experimental conditions used for these analyses were the same as previously described hereinbefore.

3. Results and discussion

The commercial Nanocyl 3100 nanotubes had a BET surface area of 320 m^2 g^{-1} and an almost neutral pH_{PZC} while the functionalized sample (MWCNT) presented an even higher surface area (S_{BET} = 439 m^2 g^{-1}) and a much lower pH_{PZC} value (pH_{PZC} = 3.0). These are expected values once the initial nanotubes were submitted to an oxidation treatment with nitric acid. It is well acknowledged that the increase of the BET surface area is mainly related to the opening of the nanotube tips and to the damage in the walls induced by the oxidation treatment. The surface areas of the supported metal catalysts were not significantly different from the support [10], in agreement with their low metal loading.

Thermodecomposition of functional groups leading to the evolution of CO_2 and CO is typically used to discriminate their chemical nature and configuration [17]. The total amount of the different oxygenated surface groups (carboxylic acids, carboxylic anhydrides, lactones, phenols, carbonyls or quinones) on carbon materials can be determined taking into consideration the amount, the decomposition temperature and the type of gas released (CO and/or CO_2). Therefore, the TPD profiles of the nanostructured support were deconvoluted into five components [17,18]: carboxylic acid groups (peak at low temperatures

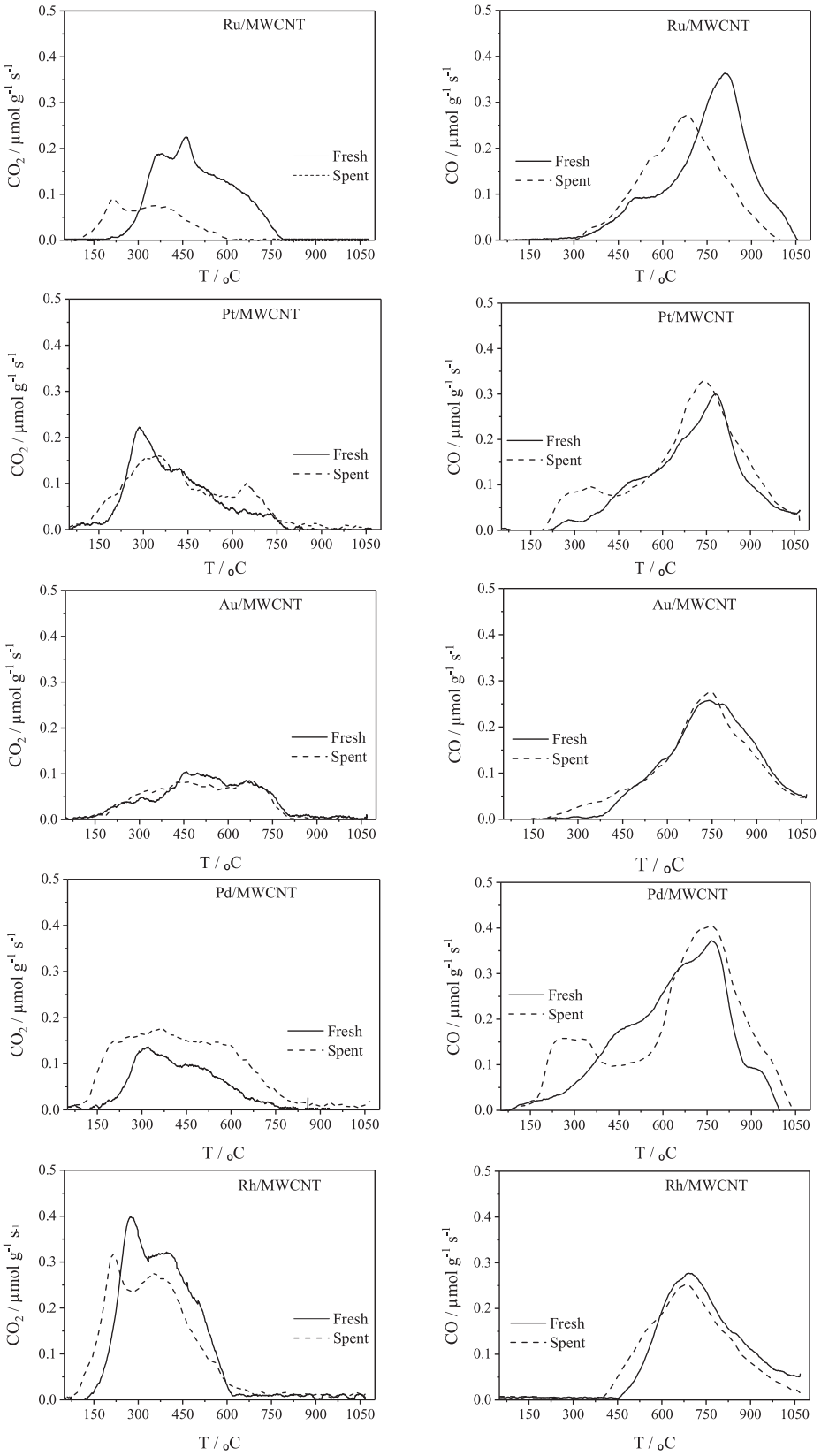

Fig. 1. CO_2 and CO profiles from TPD analyses of the fresh and spent 1D multiwalled carbon nanotube-supported noble metal catalysts.

(T < 450 °C) in the CO_2 profile), carboxylic anhydrides (peak at intermediate temperatures (400 < T < 600 °C) in both the CO and CO_2 profiles), lactones (peak at high temperatures (550 < T < 800 °C) in the CO_2 profile), phenols (peak at intermediate temperatures (550 < T < 800 °C) in the CO profile) and carbonyl-quinone groups (peak at high temperatures (750 < T < 1100 °C) in the CO profile).

The original Nanocyl 3100 nanotubes were seen not to possess a significant amount of oxygenated surface groups [10], releasing only

Table 1
CO_2 and CO amounts released during TPD analyses and D/G Raman ratios for the fresh and spent supported 1D catalysts.

Catalysts	Fresh			Spent		
	CO_2[a] (μmol g^{-1})	CO[a] (μmol g^{-1})	D/G	CO_2[a]	CO[a]	D/G
Ru/MWCNT	769	1426	3.85	274	860	3.70
Pt/MWCNT	657	1156	2.76	740	1421	2.45
Au/MWCNT	499	1129	2.89	471	1138	3.55
Pd/MWCNT	552	1660	2.50	1055	1932	3.01
Rh/MWCNT	1287	1061	3.11	1196	1008	3.60
MWCNT	767	1516	2.89	n.d.[b]	n.d.[b]	3.53
Nanocyl 3100	23	200	2.29	n.d.[b]	n.d.[b]	2.81

[a] ± 20 μmol g^{-1}.
[b] Not determined.

23 μmol g^{-1} as CO_2 and 200 μmol g^{-1} as CO. On the other hand, the MWCNT sample, which was oxidized with HNO_3, presented a high density of oxygen-containing surface groups, particularly carboxylic acids (548 μmol g^{-1}), released as CO_2. Moreover, minor amounts of carboxylic anhydrides (160 μmol g^{-1}) and lactones (65 μmol g^{-1}) were also detected. That means that the oxidation pre-treatment was effective in modifying the surface of the nanotubes, generating predominantly acidic sites.

The TPD profiles of the fresh catalysts are depicted in Fig. 1 and the total amounts of CO_2 and CO released upon thermodecomposition are compiled in Table 1.

Different amounts of CO and CO_2 were detected after the impregnation, calcination and reduction of the metals in all the nanostructured catalysts when compared to the functionalized starting support (MWCNT). It has been demonstrated that the chemical properties of the carbon surface may be modified during the impregnation step depending on the different metal precursors used and also during the thermal treatments applied during the preparation [9,19,20]. In this work, low temperatures were used (generally below 200 °C) during the preparation stage of the catalysts and, therefore, only the less stable functional groups created during the functionalization with nitric acid (mainly some carboxylic acids) were removed during the heat treatment [9,10]. In the case of the catalyst Au/MWCNT, which was the only sample treated at higher temperature (350 °C), the TPD profiles presented almost no release of CO_2 and CO up to the treatment temperature used, and consequently the lowest total amount of surface groups.

Raman spectra collected within 1000–1800 cm^{-1} for all fresh samples (Fig. 2) showed two bands at around 1560–1590 (G band) and 1320–1360 cm^{-1} (D band), which are associated with sp2 hybridization of carbon [21]. The presence of D-band indicates a certain concentration of defects since it is known that this band results from structural disordering in carbon based materials [22]. On the other hand, the G-band rises from the in-plane vibration of the C—C bonding and is very sensitive to strain effects caused by the curvature of the nanotubes, which also leads to multiple peaks in this region of the spectrum. This is probably the origin of the slight split observed at around 1600 cm^{-1} resulting in the presence of the D' band, also called 2 G band [23]. By comparing the spectra of the functionalized nanotubes to that from the original commercial sample, it was seen that Raman bands were less intense and broader. This trend has already been observed before [24] and is a consequence of the partial oxidation of the walls of the nanotubes.

Indeed, comparing the D/G ratios before and after acid treatment (Table 1), it is easy to understand the effect of the functionalization process, which creates more disorder in the nanotubes structure. As for the metal modified samples, differences in D/G ratios are also observed and they were found to be roughly related to the changes in the oxygen-containing functional groups as determined by TPD. The existence of a correlation between disordered structures as measured by D/G

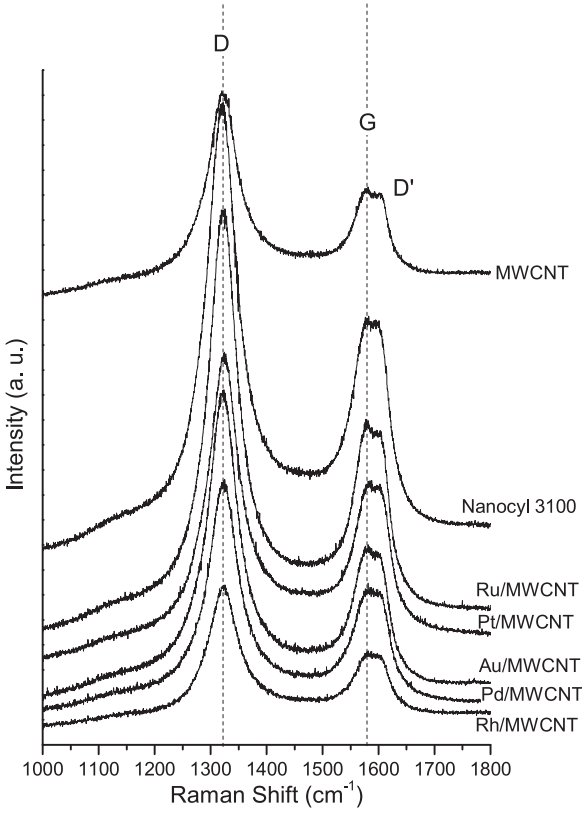

Fig. 2. Raman spectra of fresh supports and catalysts.

calculations and oxygen functionality on carbon materials has indeed been recently suggested [25]. Therefore, the Raman results presented in this study also indicate relevant modifications on the surface chemistry of the nanotubes catalyst upon impregnation.

Morphological analysis by TEM allowed estimating the distribution of metal nanoparticles on MWCNT surface (Fig. S1). Ru and Pt exhibited the smallest particles (1–2 nm) while Pd was seen to form metal clusters with few nanoparticles. Au/MWCNT presented the largest nanoparticles with an average size of 10 nm.

Liquid-phase xylose processing was performed to evaluate the behavior of these 1D nanocatalysts. A wide range of compounds may be formed through distinct reactions catalyzed by either acidic or metal sites co-existing on the surface of the studied catalysts. The very simplified reaction network depicted in Fig. 3 indicates the isomerization of xylose to xylulose and their dehydration to furfural, both reactions being well known to proceed on acidic centers [12,14,16,26–28]. Due to the presence of metal sites in a reductive atmosphere (molecular hydrogen pressure), hydrogenation of xylose/xylulose to xylitol and furfural to furfuryl alcohol are also two other possible reaction routes. Lastly, the reduction of the furanic ring in furfural and/or furfuryl alcohol leading to tetrahydrofurfural and tetrahydrofurfuryl alcohol can also be considered.

Firstly, control experiments were carried out with neat commercial Nanocyl 3100 and oxidized MWCNT samples. It was found that the nanotubes alone, without any metal sites, present no or low activity on xylose conversion as depicted in the time-dependent conversion curves in Fig. 4. Indeed the original commercial sample (Nanocyl 3100) barely reached 5% conversion within 6 h while xylose consumption was more significant, around 10%, over oxidized counterpart (MWCNT) after the same time frame. This data discloses the activity of the acidic sites created upon nitric acid functionalization. Accordingly, furfural and furfuryl alcohol, whose formation demands acidic centers, were the only products formed on MWCNT (Fig. S2).

All noble metal-based 1D catalysts, on the other hand, were clearly

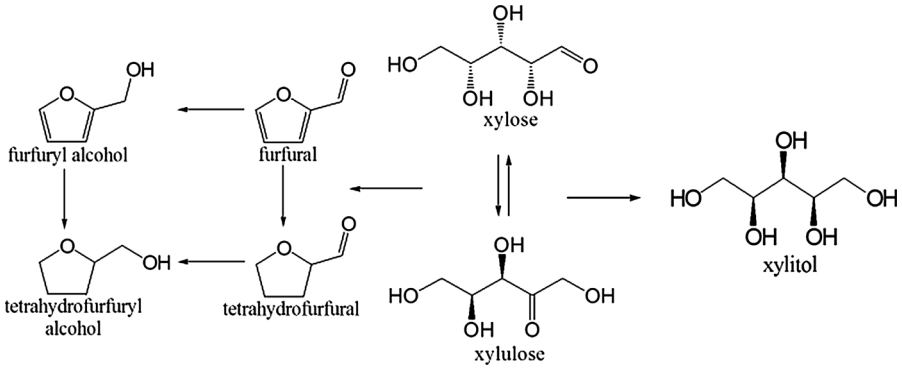

Fig. 3. Simplified network of possible reactions on acidic and metal surface sites.

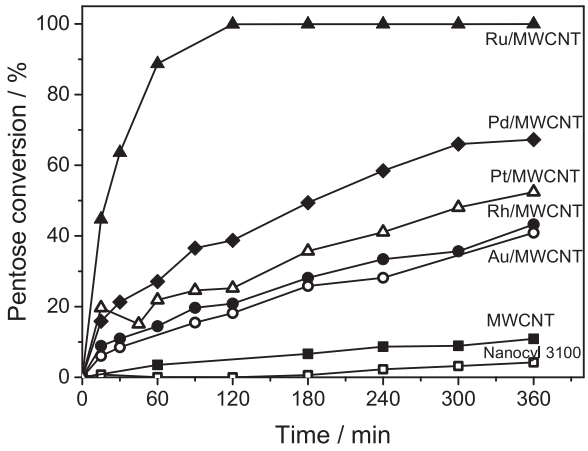

Fig. 4. Time course for the conversion of xylose on 1D multiwalled carbon nanotube-supported noble metal catalysts.

active in the liquid-phase chemoconversion of xylose as it can be seen in the time-course curves also displayed in Fig. 4. Nevertheless, marked differences were appreciated in their global activity according to the noble metal in the catalyst formulation. Ru decorated MWCNT was by far the most active catalyst with total xylose consumption within the first 1.5 h. Contrastingly, Rh and Au supported samples could barely accomplish 40% conversion after 6 h. The activity order Ru > > Pd > Pt > Rh ~ Au could indeed be established among the studied samples.

As concerning product distribution, the MWCNT-supported catalysts behaved alike and xylitol and furfuryl alcohol were the only products formed as revealed by the data collected in Fig. 5 and Table 2. It is important to mention that carbon balance was always higher than 95% (Fig. 5), substantiating the preferential formation of those two C5 chemicals. Xylose isomerization to its ketopentose form was also seen to occur on all nanostructured catalysts investigated herein, which is in agreement with previous report on which the production of xylose-derived compounds are claimed to go through xylulose as well [12,14,16,27,28]. Typical interdependent curves were indeed registered, evidencing that xylulose is an intermediate sugar on xylose conversion (Fig. S3). Therefore, the activity, selectivity and yield reported hereinafter were determined on pentoses (xylose + xylulose) molar basis.

Xylitol derived from the straight hydrogenation of the pentose aldehydes over metal sites was invariably the key product formed, accomplishing selectivities within 70–85%, which suggests that the metal centers are mostly acting independently. This data are in line with some other results in the literature [29,30]. The formation of xylitol is claimed to be a consequence of the surface reaction between adsorbed xylose (through its carbonyl group) and dissociatively chemisorbed hydrogen.

However, formation of furfuryl alcohol as the second major product is also observed. It is associated with the cooperative activity of the acidic sites as discussed before. It should be noted that no furfural was detected whatsoever on supported metal samples though. This finding indicates that pentose dehydration and furfural hydrogenation reactions possess comparable rates on these studied 1D catalysts. Taken together, these results suggest a cooperative role between some metal centers and those acidic sites created by nitric acid surface oxidation. In that way, dehydration of pentoses on acidic sites proceeds as a first step followed by the immediate hydrogenation of the intermediate furfural to furfuryl alcohol on metal sites. Such tandem cascade behavior is in close agreement with previous reports on 3D sulfated oxide-based catalysts [14] and mesostructure-architected samples [12]. It should also be mentioned that no formation of open ring products was detected, as expected, since it is reported that this reaction occurs only at temperatures above 250 °C [31]. Finally, it should be highlighted that Rh and Pd-based catalysts were the ones reaching the highest selectivities to furfuryl alcohol, up to ~20%, which is in line with their highest concentration of acidic sites as determined by TPD (Table 1). Moreover, it has been reported that the hydrogenation of carbonyl groups in furfural on these two noble metals are kinetically more favored than the straight reduction of xylose [31]. It is worth mentioning that no relevant amount of low carbon chain polyalcohols, such as glycerol and ethylene glycol, were identified over these multiwalled carbon nanotubes-supported noble metal catalysts, contrasting the performance of Ni-based catalysts reported elsewhere [13,32].

The spent catalysts were recovered by filtration right after reaction, dried and characterized as regarding their surface chemistry, since it might endure foremost changes upon aqueous-phase processing conditions. It was thus assessed by TPD and the CO_2 and CO profiles are contrasted to those from fresh samples in Fig. 1. The total amounts of gases released from the spent catalysts are also summarized in Table 1.

Significant amounts of the functional surface groups were still detected on the spent 1D catalysts, revealing their stability under the operation conditions used during the xylose conversion. Actually, oxygenated surface groups were found practically unaffected after exposure to hot pressurized liquid water when compared to the fresh catalysts (Fig. 1). The exception is the spent Ru/MWCNT catalysts, for which it can be observed that the amounts of CO and CO_2 released are lower than those from the fresh catalyst (Table 1).

Generally, it can be observed that CO_2 is released in a broader range of temperatures and that CO starts to evolve at lower temperatures. For the spent Pt/MWCNT and Pd/MWCNT catalysts a peak at low temperatures (200–400 °C) in the CO profile can be clearly observed, which does not appear as noticeable in the remaining samples. The differences in these profiles might be related to some reaction products adsorbed on the catalyst surface. These adsorbed species may contribute for the lower activity of the Pd and Pt catalysts compared to Ru/MWCNT since they can partially block the access of the reactants to the catalytic active surface sites.

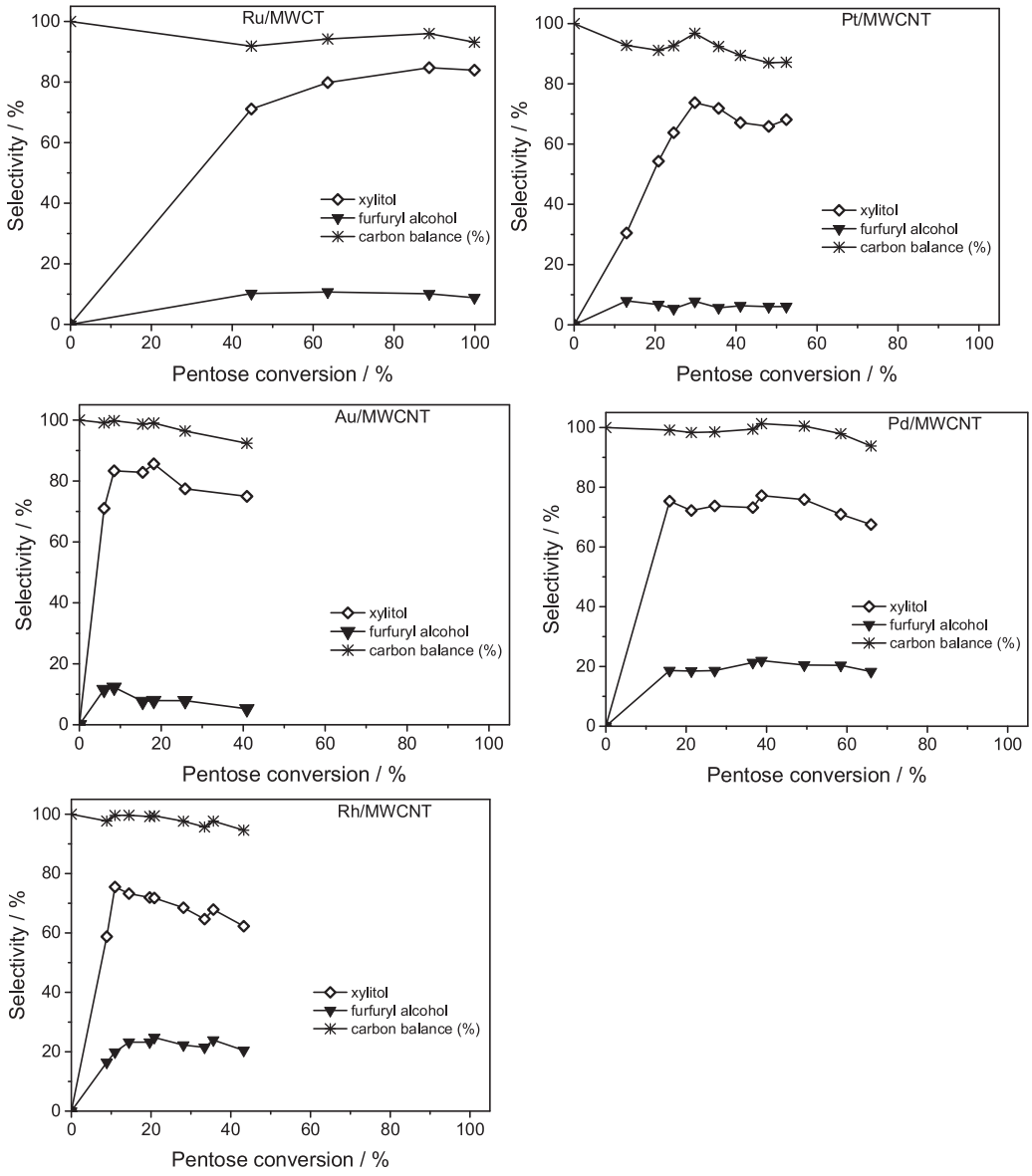

Fig. 5. Selectivity to xylitol and furfuryl alcohol as a function of pentose conversion on 1D multiwalled carbon nanotube-supported noble metal catalysts.

Table 2
Xylose conversion (X), selectivity to xylitol (S_{XOL}) and furfuryl alcohol (S_{FFA}) and yield to xylitol (Y_{XOL}) and furfuryl alcohol (Y_{FFA}) on 1D multiwalled carbon nanotube-supported noble metal catalysts.

Catalysts	X[a] (%)	S_{XOL}[b] (%)	S_{FFA}[b] (%)	Y_{XOL}[c] (%)	Y_{FFA}[c] (%)
Ru/MWCNT	100	71	10	84	9
Pt/MWCNT	52	67	6	35	3
Au/MWCNT	41	75	5	31	2
Pd/MWCNT	66	77	22	45	12
Rh/MWCNT	43	62	20	27	9
MWCNT[d]	11	0	90	0	10

[a] Conversion after 6 h reaction.
[b] Selectivity at isoconversion (~40%).
[c] Yield after 6 h reaction.
[d] Data at 11% conversion – the highest conversion after 6 h reaction. Furfural was also produced with selectivity of 10%.

Raman spectra of spent catalysts were also collected (Fig. S4) and the D/G ratios are summarized in Table 1. While the spectra were qualitatively alike, the calculated D/G ratios were generally higher for all spent catalysts. This fashion indicates a more significant presence of amorphous carbonaceous species on the 1D catalysts after reaction. It might be bound to the presence of reaction products on catalyst surface, in close agreement with the results from TPD discussed previously.

The original results presented herein demonstrated the potential application of 1D catalysts prepared from metal particles supported on functionalized multiwalled carbon nanotubes on pentose valorization. Xylitol, an important industrial sweetener in the food industry, can be obtained in high carbon yields (~85%) on Ru-based catalyst (Table 2). It was also revealed a potential cooperative activity between metal and oxygen-containing acidic surface sites since a qualitative correlation between the occurrence of such site and the formation of furfuryl alcohol was seen. This finding indicates that the assembly of the acidic and metal sites on the catalyst surface can have great relevance on designing bifunctional catalysts for aqueous-phase biomass conversion.

4. Conclusions

The use of 1D multiwalled carbon nanotubes to synthesize nanostructured catalysts is highly potential due to the chemically very active surface on which a multitude of functional groups can be generated. Supporting noble metals on them rendered active catalysts for xylose

conversion. Ru was the most active metal on xylose direct hydrogenation to xylitol, providing 85% yield. Despite being xylitol the major product formed on all noble metals, furfuryl alcohol was also produced at promising yields on Pd and Rh-based catalysts. This behavior was found to be related to the concentration of oxygen-containing acidic sites on the surface of multiwalled nanotubes as generated by nitric acid pre-treatment. The existence of vicinal metal and acidic sites is claimed to promote the tandem reactions from xylose to furfuryl alcohol. The catalysts revealed to be stable on aqueous-phase processing of xylose, retaining their acid surface sites after 6 h.

Acknowledgements

The authors acknowledge CNPq and FAPERJ (Brazil) and NORTE 2020, FEDER under Program PT2020 (Project AIProcMat@N2020 – Advanced Industrial Processes and Materials for a Sustainable Northern Region of Portugal 2020″, with the reference NORTE-01-0145-FEDER-000006) and FCT and FEDER, under Program COMPETE2020 (Project POCI-01-0145-FEDER-006984) (Portugal) for financial support. R.F.P. thanks CAPES (Brazil) for his PhD scholarship.

Appendix A. Supplementary data

Supplementary material related to this article can be found, in the online version, at doi:https://doi.org/10.1016/j.apcatb.2018.03.042.

References

[1] R.M. Ravenelle, J.R. Copeland, W.G. Kim, J.C. Crittenden, C. Sievers, ACS Catal. 1 (5) (2011) 552–561.
[2] R.M. Ravenelle, J.R. Copeland, A.H. Van Pelt, J.C. Crittenden, C. Sievers, Top. Catal. 55 (2012) 162–174.
[3] R.M. Ravenelle, F. Schüßler, A. D'Amico, N. Danilina, J.A. van Bokhoven, J.A. Lercher, C.W. Jones, C. Sievers, J. Phys. Chem. C 114 (46) (2010) 19582–19595.
[4] E.M. Albuquerque, L.E.P. Borges, M.A. Fraga, C. Sievers, ChemCatChem 14 (2017) 2675–2683.
[5] Y. Yan, J. Miao, Z. Yang, F.-X. Xiao, H.B. Yang, B. Liu, Y. Yang, Chem. Soc. Rev. 44 (2015) 3295–3346.
[6] J.L. Figueiredo, M.F.R. Pereira, P. Serp, J.L. Figueiredo (Eds.), Carbon Materials for Catalysis, John Wiley & Sons, Inc., Hoboken, NJ, 2009, pp. 177–217.
[7] P. Serp, M. Corrias, P. Kalck, Appl. Catal. A 253 (2003) 337–358.
[8] R.P. Rocha, J.P.S. Sousa, A.M.T. Silva, M.F.R. Pereira, J.L. Figueiredo, Appl. Catal. B 104 (2011) 330–336.
[9] A. Sepulveda-Escribano, F. Coloma, F. Rodriguez-Reinoso, Appl. Catal. A 173 (1998) 247–257.
[10] O.S.G.P. Soares, J.J.M. Orfao, M.F.R. Pereira, Ind. Eng. Chem. Res. 49 (2010) 7183–7192.
[11] A.G. Gonçalves, J.L. Figueiredo, J.J.M. Órfão, M.F.R. Pereira, Carbon 48 (2010) 4369–4381.
[12] S.J. Canhaci, R.F. Perez, L.E.P. Borges, M.A. Fraga, Appl. Catal. B 207 (2017) 279–285.
[13] R. Morales, C.H. Campos, J.L.G. Fierro, M.A. Fraga, G. Pecchi, RSC Adv. 6 (2016) 67817–67826.
[14] R.F. Perez, S.J. Canhaci, L.E.P. Borges, M.A. Fraga, Catal. Today 289 (2017) 273–279.
[15] E.G. Rodrigues, S.A.C. Carabineiro, J.J. Delgado, X. Chen, M.F.R. Pereira, J.J.M. Órfão, J. Catal. 285 (2012) 83–91.
[16] R.F. Perez, M.A. Fraga, Green Chem. 16 (2014) 3942–3950.
[17] J.L. Figueiredo, M.F.R. Pereira, M.M.A. Freitas, J.J.M. Orfão, Carbon 37 (1999) 1379–1389.
[18] J.L. Figueiredo, M.F.R. Pereira, M.M.A. Freitas, J.J.M. Órfão, Ind. Eng. Chem. Res. 46 (2007) 4110–4115.
[19] H.E. Vandam, H. Van Bekkum, J. Catal. 131 (1991) 335–349.
[20] M.A. Fraga, E. Jordão, M.J. Mendes, M.M.A. Freitas, J.L. Faria, J.L. Figueiredo, J. Catal. 209 (2002) 355–364.
[21] R. Vidano, D.B. Fischbach, J. Am. Ceram. Soc. 61 (1978) 13–17.
[22] M.S. Dresselhaus, A. Jorio, M. Hofmann, G. Dresselhaus, R. Saito, Nano Lett. 10 (2010) 751–758.
[23] S. Vollebregt, R. Ishihara, F.D. Tichelaar, Y. Hou, C.I.M. Beenakker, Carbon 50 (2012) 3542–3554.
[24] E. Arici, S. Karazhanov, Mater. Sci. Semicond. Proc. 41 (2016) 137–149.
[25] Y. Gao, K. Xie, S. Mi, N. Liu, W. Wang, W. Huang, Int. J. Hydrogen Energy 38 (2013) 16665–16676.
[26] V. Choudhary, A.B. Pinar, S.I. Sandler, D.G. Vlachos, R.F. Lobo, ACS Catal. 1 (2011) 1724–1728.
[27] V. Choudhary, S.I. Sandler, D.G. Vlachos, ACS Catal. 2 (2012) 2022–2028.
[28] V. Choudhary, S. Caratzoulas, D.G. Vlachos, Carbohydr. Res. 368 (2013) 89–95.
[29] J. Mikkola, T. Salmi, R. Sjölm, J. Chem, Technol. Biotechnol. 76 (2001) 90–100.
[30] M. Yadav, D.K. Mishra, J. Hwang, Appl. Catal. A 425–426 (2012) 110–116.
[31] J. Lee, Y. Xub, G. Huber, Appl. Catal. B 140 (2013) 98–107.
[32] R. Morales, C.H. Campos, J.L.G. Fierro, M.A. Fraga, G. Pecchi, Mol. Catal. 436 (2017) 182–189.